Chiral Spin-Chain Interfaces Exhibiting Event-Horizon Physics

Matthew D. Horner, Andrew Hallam, and Jiannis K. Pachos
School of Physics and Astronomy, University of Leeds, Leeds LS2 9JT, United Kingdom

(Received 25 July 2022; revised 28 September 2022; accepted 14 December 2022; published 3 January 2023)

The interface between different quantum phases of matter can give rise to novel physics, such as exotic topological phases or nonunitary conformal field theories. Here we investigate the interface between two spin chains in different chiral phases. Surprisingly, the mean field theory approximation of this interacting composite system is given in terms of Dirac fermions in a curved space-time geometry. In particular, the interface between the two phases represents a black hole horizon. We demonstrate that this representation is faithful both analytically, by employing bosonization to obtain a Luttinger liquid model, and numerically, by employing matrix product state methods. A striking prediction from the black hole equivalence emerges when a quench, at one side of the interface between two opposite chiralities, causes the other side to thermalize with the Hawking temperature for a wide range of parameters and initial conditions.

DOI: 10.1103/PhysRevLett.130.016701

Many quantum lattice models exhibit emergent relativistic physics in their continuum limit. The celebrated example is graphene whose low-energy regime is described by the Dirac equation [1,2]. Other examples admitting relativistic descriptions are Kitaev's honeycomb model [3,4], superconductors [5,6], and the XX model [7,8]. The relativistic description of these systems opens up the possibility to simulate curved spacetimes in the laboratory.

Here we modify the 1D spin-$1/2$ XX model with a three-spin chiral interaction, making the system interacting. Such chiral systems exhibit a rich spectrum of quantum correlations [9] and give rise to skyrmionic configurations [10]. We show these chiral systems are effectively modeled by the Dirac equation on a curved spacetime. This gives the possibility to realize a black hole background.

The emergent black hole is revealed by applying the mean field (MF) approximation. We test the validity of this approximation through a detailed analysis of the phase diagram and a comparison with the full spin model. We model the spin model numerically with matrix product state (MPS) techniques, and analytically through bosonization. We find the MF approximation faithfully predicts a phase transition between a chiral and nonchiral phase. Remarkably, the emergent event horizon aligns precisely with chiral phase interfaces. The inside of the black hole corresponds to a chiral region with a central charge of $c = 2$, while the outside corresponds to a nonchiral region with a central charge of $c = 1$.

To verify the emergent black hole, we investigate whether it can reproduce the Hawking effect. Hawking radiation is generated by vacuum fluctuations of quantum fields near the horizon of a black hole, which causes the black hole to evaporate [11,12]. Here, we simulate a Hawking-like effect by quenching the MF system. This causes a wave packet to tunnel across the horizon and escape into the outer region, with a thermal distribution at the Hawking temperature. This alternative mechanism was originally derived in Ref. [13] and is used to simulate Hawking radiation in fermionic lattice models [14–29]. We demonstrate this for a variety of quenches. As the emergent geometry is generated from the couplings, it is fixed with no black hole evaporation or backreaction of matter on the geometry.

Our investigation shows horizon physics can model chiral interfaces and accurately predicts the evolution of interacting chiral phases across a phase interface. We envision that the geometry provides an elegant formalism to model strongly interacting systems and their interfaces in higher dimensions.

Consider a periodic chain of N spin-$1/2$ particles with Hamiltonian

$$H = \sum_{n=1}^{N} \left[-\frac{u}{2}(\sigma_n^x \sigma_{n+1}^x + \sigma_n^y \sigma_{n+1}^y) + \frac{v}{4}\chi_n \right], \tag{1}$$

where u, $v \in \mathbb{R}$, $\{\sigma_n^x, \sigma_n^y, \sigma_n^z\}$ are the Pauli matrices of the nth spin and χ_n is the spin chirality given by the three-spin interaction

$$\chi_n = \boldsymbol{\sigma}_n \cdot \boldsymbol{\sigma}_{n+1} \times \boldsymbol{\sigma}_{n+2}, \tag{2}$$

where $\boldsymbol{\sigma}_n$ is the vector of Pauli matrices of the nth spin [9,30]. The chirality operator is a measure of the solid angle spanned by three neighboring spins.

The model of Eq. (1) can be mapped to an interacting fermionic Hamiltonian via a Jordan-Wigner transformation. After application of self-consistent MF theory to Eq. (1) (see Supplemental Material [31]) we obtain

$$H_{\mathrm{MF}} = \sum_{n=1}^{N} \left(-u c_n^\dagger c_{n+1} - \frac{iv}{2} c_n^\dagger c_{n+2} \right) + \mathrm{H.c.} \tag{3}$$

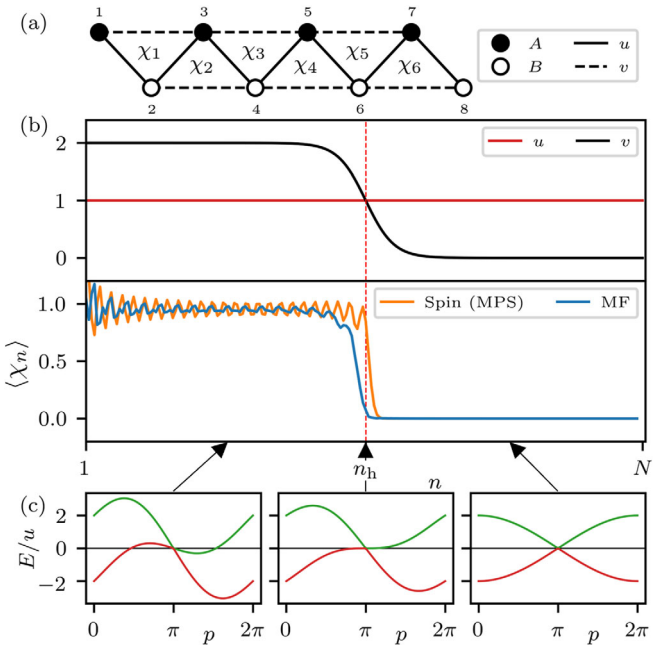

FIG. 1. (a) The couplings of the Hamiltonian of Eq. (3) with diatomic coloring, A and B. The chirality operator, χ_n, is defined for each triangular plaquette. (b) An example of interface profile for the couplings u and v with the corresponding ground state chirality, $\langle\chi_n\rangle$. The system changes from a chiral phase, $\langle\chi_n\rangle \neq 0$, when $|v| > |u|$, to nonchiral phase, $\langle\chi_n\rangle = 0$, when $|v| < |u|$, across the interface, n_h, corresponding to the event horizon in the continuum theory. The chirality is determined by mean field (MF) theory and by numerical modeling of the spin chain (DMRG with bond dimension $D = 400$) for system size $N = 200$. (c) The mean field dispersion relations are obtained from a diatomic representation (see Supplemental Material). The sign of v determines the direction the cones tilt.

This free Hamiltonian is diagonalized exactly with a Fourier transform giving a gapless dispersion with unequal left- and right-moving Fermi velocities.

By introducing two sublattices, A and B, as shown in Fig. 1(a), the Brillouin zone folds giving two bands as shown in Fig. 1(c). There is a Dirac cone located at $p_0 = \pi$, which tilts as v is increased. For $|v| < |u|$ we have a type-I Weyl fermion with a single Fermi point; for $|u| = |v|$ we have critical tilting giving rise to a type-III Weyl fermion, with one flat band; and for $|v| > |u|$ the cone overtilts, corresponding to type-II Weyl fermions [14–16]. For $|v| > |u|$, additional Fermi points appear due to the Nielsen-Ninomiya theorem [32,33]. This reveals the emergent relativistic dispersion at low energy.

To reveal the geometric description we derive the corresponding continuum limit. The continuum limit is found by Taylor expanding H_{MF} in momentum space about p_0, the Fermi point where $E(p_0) = 0$, to first order in p [4,6,34]. This yields a Dirac Hamiltonian on a $(1+1)$D spacetime with metric

$$ds^2 = \left(1 - \frac{v^2}{u^2}\right)dt^2 - \frac{2v}{u^2}dtdx - \frac{1}{u^2}dx^2, \tag{4}$$

which is the Gullstrand-Painlevé metric of a black hole [35]. If v is upgraded to a sufficiently slowly varying function $v(x)$, such as in Fig. 1(b), then this continuum description remains valid and an event horizon is located at the critical point x_h, where $|v(x_h)| = |u|$, which corresponds to the location of critical tilt in Fig. 1(c). This is a background metric fixed by the couplings, with no backreaction of the field on the spacetime. From the metric, the corresponding Hawking temperature is [16]

$$T_H = \frac{1}{2\pi}\left|\frac{dv(x_h)}{dx}\right|. \tag{5}$$

Therefore, the original spin model of Eq. (1) with inhomogeneous couplings is effectively described by free fermions on a fixed $(1+1)$D black hole background [14–16,35].

Before proceeding with the black hole analogy, we first establish how accurate the MF approximation is by studying the phase diagram of Eq. (1) for homogeneous u and v. The MF Hamiltonian Eq. (3) reveals that for $v < u$ the system is in a disordered, gapless, XX phase, while as v increases it passes through a second-order phase transition into a gapless chiral phase, corresponding to a nonzero ground state chirality $\langle\chi_n\rangle$, as Fig. 2(a) shows, so chirality is an order parameter. The MF chiral phase transition is located at $|v| = |u|$, coinciding with the critical tilting of the Dirac cones and the appearance of additional Fermi points, as Fig. 1(c) shows. Near the critical point,

$$\langle\chi_n\rangle \sim (v - v_c)^{\gamma}, \tag{6}$$

with critical point $v_c = u$ and critical exponent $\gamma = 1$. Moreover, using finite density matrix renormalization group (DMRG) [36] we estimate the critical point of the spin model of Eq. (1) is at $v_c \approx 1.12u$ with a critical exponent $\gamma \approx 0.39$. A comparison between the chirality of the spin model and the MF model for inhomogeneous and homogeneous couplings can be seen in Figs. 1(b) and 2(a), respectively, revealing the effectiveness of MF.

To gain further insight into the chiral phase transition, we consider the behavior of the entanglement entropy as v is increased. As the model is gapless for all v, it can be described by a conformal field theory (CFT). Therefore, the ground state entanglement entropy of a partition of $L \ll N$ spins should follow

$$S_L = \frac{c}{3}\ln L + S_0, \tag{7}$$

where $c \in \mathbb{Z}$ is the central charge of the CFT and S_0 is a constant [37]. Using this formula, we estimate c as a function of v for the full spin model and the MF. In Fig. 2(b) we

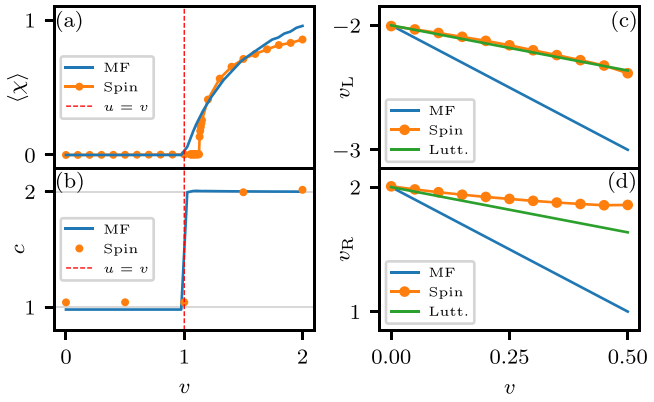

FIG. 2. (a) The average ground state chirality, $\langle\chi\rangle = \sum_n \langle\chi_n\rangle/N$, for the mean field (MF) model ($N = 500$) and spin model found using DMRG ($N = 200$, $D = 300$) where $u = 1$. (b) The central charge, c, obtained for the MF model ($N = 500$) and the spin model found using DMRG ($v \leq u$: $N = 200$, $D = 300$ and $v > u$: $N = 160$, $D = 800$). (c),(d) The Fermi velocities, v_L and v_R, respectively, ($u = 1$) derived from the mean field (MF) and Luttinger liquid descriptions compared to the numerical results of the MPS excitation ansatz for the spin model at bond dimension $D = 36$ in the thermodynamic limit.

see that $c \approx 1$ in the XX phase and $c \approx 2$ in the chiral phase, with good agreement between the MPS and MF results. We can clearly interpret this in the MF model: the additional Fermi points appearing when $|v| > |u|$, as Fig. 1(c) shows, cause the model to transition from a $c = 1$ CFT with a single Dirac fermion to a $c = 2 = 1 + 1$ CFT with two Dirac fermions, as each zero-energy crossing contributes one half of a Dirac fermion. This can also be understood from the lattice structure of the MF model, as Fig. 1(a) shows, where for $|v| \ll |u|$ a single zigzag fermionic chain dominates ($c = 1$) while for $|v| \gg |u|$ two fermionic chains dominate, corresponding to the edges of the ladder, thus effectively doubling the degrees of freedom ($c = 2$).

The MF faithfully reproduces many features of the full model, especially for $|v| < |u|$ suggesting the interactions are not significant here. We now investigate the validity of the MF analytically by bosonizing the spin Hamiltonian for the $|v| < |u|$ phase, and employing Luttinger liquid theory as an alternative derivation of the Fermi velocities of the model [38–40]. After a Jordan-Wigner transformation, the spin Hamiltonian takes the form $H = H_{\mathrm{MF}} + H_{\mathrm{int}}$, where H_{MF} is the quadratic MF Hamiltonian of Eq. (3) and H_{int} is an interaction term containing quartic terms. For $|v| < |u|$, the single-band dispersion of the MF Hamiltonian Eq. (3) suggests the spin model has two Fermi points located at $p_{R,L} = \pm\pi/2$, with Fermi velocities $v_{R,L} = 2(\pm u - v)$. By expanding around these Fermi points and bosonizing the interaction terms using the methods of [38–40], the fully interacting Hamiltonian is mapped to the free boson Hamiltonian

$$H = u \int dx[\Pi^2 + (\partial_x \Phi)^2], \tag{8}$$

where the fields obey the canonical commutation relations $[\Phi(x), \Pi(y)] = i\delta(x - y)$. The interactions rescale the Fermi velocities $v_{R,L} \to v'_{R,L} = 2[\pm u - v(1 - 2/\pi)]$, but leave the Luttinger parameter unchanged at $K = 1$ (see Supplemental Material), suggesting the model remains a noninteracting free fermion model.

The dispersion of the spin model as a function of v for $|v| < |u|$ can be calculated using the MPS excitation ansatz working in the thermodynamic limit [41]. This dispersion features unequal left- and right-moving Fermi velocities whose magnitudes change oppositely with v which is the signature of tilting of the cones similar to the MF. In Figs. 2(c) and 2(d), the Fermi velocities $v_{L,R}$ obtained from the MF, the Luttinger liquid model and the spin Hamiltonian are compared. The Luttinger liquid model is more accurate than MF. We expect the disagreement to be lifted at higher order in perturbation theory.

We now study the emergent black hole. It has been shown that many analogue gravitational systems will exhibit a Hawking-like effect, whereby emission of radiation is described by scattering events following a thermal distribution at the Hawking temperature [14–28] which is the definition of the Hawking effect we use. Reversing the argument, we investigate whether the Hawking effect can describe quenched time evolutions across the chiral interface. To simulate large system sizes and long evolution times, we resort to the MF of Eq. (3) rather than the full spin model. Consider an open, inhomogeneous system with couplings $u(x) = 1$ and

$$v(x) = \alpha \tanh[\beta(x - x_h)], \tag{9}$$

where $\alpha, \beta \in \mathbb{R}$ and x_h is in the center of the system. Here, x is the unit cell coordinate in order to align with our continuum conventions (see Supplemental Material). This produces a positive and negative chiral region separated by a small zero-chirality region in between. In the continuum limit, this corresponds to a black hole–white hole interface. This is a common setup used in the literature, see Refs. [19,25,42].

Following the method of Ref. [17], we initialize a single-particle state $|n_0\rangle = c^\dagger_{n_0}|0\rangle$ on the n_0th lattice site inside the left half of the system, and let the wave function evolve across the interface into the other half with the Hamiltonian H_{MF}, as shown in Fig. 3(a). We measure the wave function overlap with energy modes that exist only on the other side of the interface as

$$P(k, t) = |\langle k|e^{-iHt}|n_0\rangle|^2, \tag{10}$$

where $|k\rangle$ are single-particle eigenstates of H_{out}, where H_{out} is the Hamiltonian of Eq. (3) truncated to the outside region. This method utilizes the result that Hawking radiation can be viewed as quantum tunneling [13], differing from the usual interpretation as vacuum fluctuations.

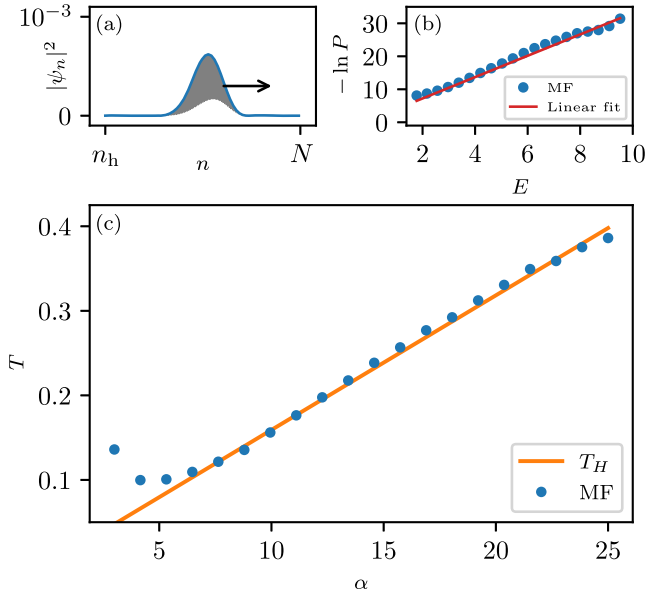

FIG. 3. (a) The lattice wave function ψ_n on the right half of the system ($n \in [n_h, N]$) transmitted through the horizon, for the couplings $u = 1$ and v given by Eq. (9) with $\alpha = 20, \beta = 0.1$, and the horizon at $n_h = N/2$ with $N = 500$. The particle tunnels across at $t \approx 2$ and a wave packet escapes which we interpret as Hawking radiation. (b) A snapshot of the overlap $-\ln P$ vs the energy of the state E at time $t = 4.5$. The system thermalizes shortly after the particle passes through the interface, displaying a linear dependence on E, where the gradient is given by $1/T$. (c) The temperature T of the radiation vs α extracted after time $t = 4.5$. T grows linearly with α close to the predictions of the Hawking formula $T_H \approx \alpha\beta/2\pi$.

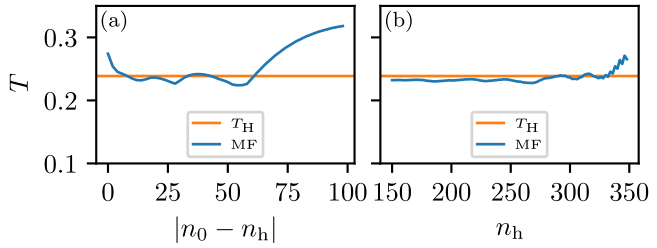

FIG. 4. (a) The measured temperature T vs the distance $|n_0 - n_h|$ from the event horizon that the particle is released for the mean field (MF) system of size $N = 500$, $\alpha = 15$, $\beta = 0.1$, and $n_h = N/2$. We see the temperature is insensitive to the initial position n_0 of the particle. This effect breaks down if n_0 is very close to the horizon or too far away, near the boundary of the system. (b) The measured temperature T vs the position of the horizon n_h for the same system, where $n_0 = n_h - 25$. The temperature is insensitive to the location of the horizon, except when it gets too close to the boundaries, in which case it breaks down.

This process will not cause the black hole to evaporate as the effective metric is fixed by the couplings.

We find numerically that interfaces between the two chiral phases thermalize the wave function: shortly after the wave function evolves across the interface, the external distribution takes the form $P(k,t) \propto e^{-E(k)/T}$, where T is some effective temperature. Figure 3(b) shows $P(k,t)$ at time $t = 4.5$ for a system with parameters $N = 500$, $n_h = 250$, $\alpha = 20$ and $\beta = 0.1$, where we prepared the particle at $n_0 = 230$. The value $\beta = 0.1$ is taken to suppress lattice and finite size effects. We see $P(k,t)$ strongly thermalizes to a Boltzmann distribution at temperature T. In Fig. 3(c), we present the dependence of T on α. We see it closely follows the Hawking formula $T_h = \alpha\beta/2\pi$, obtained from Eqs. (5) and Eq. (9), for a wide range of couplings, α, thus accurately modeling the physics of the chiral interface. The thermalization to T_h breaks down when $\alpha < 4$ as the couplings are not sharp enough to provide a sufficient interface, whereas for large α the couplings vary too fast for the continuum approximation to be valid, which is where the black hole physics emerges.

We observe strong thermalization for the chiral-nonchiral interface, corresponding to a single horizon, such as in Fig. 1. However, this system does not thermalize to the Hawking temperature as closely as the black hole–white hole interface as it requires larger system sizes and times than we had numerical access too [18]. Nevertheless, the system only thermalizes if it contains a phase interface, or equivalently an event horizon (see Supplemental Material).

The Hawking temperature $T_H = \alpha\beta/2\pi$ is a simple formula that describes a complex thermalization process. It does not depend on the position of the quench, n_0, nor the horizon location, n_h. To verify this numerically, we study the dependence of T on n_0 [Fig. 4(a)] and n_h [Fig. 4(b)]. We see T is largely insensitive to the initial conditions and only fails if n_0 is too close or too far away from the interface, or when the interface n_h is too close to the system edges. In all these cases boundary effects contribute and the exterior region which the overlap $P(k,t)$ is measured in becomes too small. These observations show that the thermalization is robust, aiding in any potential experimental realization. We stress this thermalization is not an equilibration to a thermal state as $t \to \infty$, but instead is an effective thermalization due to short time-scale scattering events [18]. As the MF is integrable, it equilibrates to a generalized Gibbs ensemble instead in the $t \to \infty$ limit [43–47] (see Supplemental Material).

In this Letter, we demonstrated that the low-energy behavior of a chiral spin chain can be described by Dirac fermions on a black hole background, where the event horizons are aligned with phase interfaces. To demonstrate the faithfulness of this we employed mean field, matrix product states and bosonization to probe the phase diagram. We simulated the Hawking effect by quenching a system containing a phase interface for a variety of quenches, interface positions, and couplings. We envision this bridge between chiral systems and event horizons can facilitate quantum simulations of Hawking radiation, e.g., with cold atom technology [24,26,48].

Moreover, our investigation opens up a way for modeling strongly correlated systems by effective geometric theories with extreme curvature, thus providing a tool for their analytical investigation.

We thank Aydin Deger, Patricio Salgado-Rebolledo, Joe Barker, and Diptiman Sen for insightful discussions. M. D. H., A. H., and J. K. P. acknowledge support by EPSRC (Grant No. EP/R020612/1). A. H. acknowledges support by the Leverhulme Trust Research Leadership Award RL-2019-015.

[1] P. R. Wallace, The band theory of graphite, Phys. Rev. **71**, 622 (1947).
[2] A. H. Castro Neto, F. Guinea, N. M. R. Peres, K. S. Novoselov, and A. K. Geim, The electronic properties of graphene, Rev. Mod. Phys. **81**, 109 (2009).
[3] A. Kitaev, Anyons in an exactly solved model and beyond, Ann. Phys. (Amsterdam) **321**, 2 (2006), January Special Issue.
[4] A. Farjami, M. D. Horner, C. N. Self, Z. Papić, and J. K. Pachos, Geometric description of the Kitaev honeycomb lattice model, Phys. Rev. B **101**, 245116 (2020).
[5] N. Read and D. Green, Paired states of fermions in two dimensions with breaking of parity and time-reversal symmetries and the fractional quantum Hall effect, Phys. Rev. B **61**, 10267 (2000).
[6] O. Golan and A. Stern, Probing topological superconductors with emergent gravity, Phys. Rev. B **98**, 064503 (2018).
[7] E. Lieb, T. Schultz, and D. Mattis, Two soluble models of an antiferromagnetic chain, Ann. Phys. (Leipzig) **16**, 407 (1961).
[8] A. De Pasquale, G. Costantini, P. Facchi, G. Florio, S. Pascazio, and K. Yuasa, Xx model on the circle, Eur. Phys. J. Spec. Top. **160**, 127 (2008).
[9] D. I. Tsomokos, J. J. García-Ripoll, N. R. Cooper, and J. K. Pachos, Chiral entanglement in triangular lattice models, Phys. Rev. A **77**, 012106 (2008).
[10] Y. Tikhonov, S. Kondovych, J. Mangeri, M. Pavlenko, L. Baudry, A. Sené, A. Galda, S. Nakhmanson, O. Heinonen, A. Razumnaya, I. Luk'yanchuk, and V. M. Vinokur, Controllable skyrmion chirality in ferroelectrics, Sci. Rep. **10**, 8657 (2020).
[11] S. W. Hawking, Particle creation by black holes, Commun. Math. Phys. **43**, 199 (1975).
[12] D. N. Page, Hawking radiation and black hole thermodynamics*, New J. Phys. **7**, 203 (2005).
[13] M. K. Parikh and F. Wilczek, Hawking Radiation as Tunneling, Phys. Rev. Lett. **85**, 5042 (2000).
[14] G. Volovik and K. Zhang, Lifshitz transitions, type-ii Dirac and Weyl fermions, event horizon and all that, J. Low Temp. Phys. **189**, 276 (2017).
[15] G. Volovik and P. Huhtala, Fermionic microstates within the Painlevé-Gullstrand black hole, J. Exp. Theor. Phys. **94**, 853 (2002).
[16] G. Volovik, Black hole and Hawking radiation by type-ii Weyl fermions, JETP Lett. **104**, 645 (2016).
[17] R.-Q. Yang, H. Liu, S. Zhu, L. Luo, and R.-G. Cai, Simulating quantum field theory in curved spacetime with quantum many-body systems, Phys. Rev. Res. **2**, 023107 (2020).
[18] D. Sabsovich, P. Wunderlich, V. Fleurov, D. I. Pikulin, R. Ilan, and T. Meng, Hawking fragmentation and Hawking attenuation in Weyl semimetals, Phys. Rev. Res. **4**, 013055 (2022).
[19] D. Maertens, N. Bultinck, and K. Van Acoleyen, Hawking radiation on the lattice as universal (Floquet) quench dynamics, arXiv:2204.06583.
[20] H. Huang, K.-H. Jin, and F. Liu, Black-hole horizon in the Dirac semimetal $Zn_2In_2S_5$, Phys. Rev. B **98**, 121110(R) (2018).
[21] H. Liu, J.-T. Sun, C. Song, H. Huang, F. Liu, and S. Meng, Fermionic analogue of high temperature Hawking radiation in black phosphorus, Chin. Phys. Lett. **37**, 067101 (2020).
[22] S. Guan, Z.-M. Yu, Y. Liu, G.-B. Liu, L. Dong, Y. Lu, Y. Yao, and S. A. Yang, Artificial gravity field, astrophysical analogues, and topological phase transitions in strained topological semimetals, npj Quantum Mater. **2**, 23 (2017).
[23] A. Retzker, J. I. Cirac, M. B. Plenio, and B. Reznik, Methods for Detecting Acceleration Radiation in a Bose-Einstein Condensate, Phys. Rev. Lett. **101**, 110402 (2008).
[24] J. Rodríguez-Laguna, L. Tarruell, M. Lewenstein, and A. Celi, Synthetic Unruh effect in cold atoms, Phys. Rev. A **95**, 013627 (2017).
[25] A. Roldán-Molina, A. S. Nunez, and R. A. Duine, Magnonic Black Holes, Phys. Rev. Lett. **118**, 061301 (2017).
[26] A. Kosior, M. Lewenstein, and A. Celi, Unruh effect for interacting particles with ultracold atoms, SciPost Phys. **5**, 61 (2018).
[27] J. Steinhauer, Observation of quantum Hawking radiation and its entanglement in an analogue black hole, Nat. Phys. **12**, 959 (2016).
[28] M. Stone, An analogue of Hawking radiation in the quantum Hall effect, Classical Quantum Gravity **30**, 085003 (2013).
[29] L. Mertens, A. G. Moghaddam, D. Chernyavsky, C. Morice, J. van den Brink, and J. van Wezel, Thermalization by a synthetic horizon, Phys. Rev. Res. **4**, 043084 (2022).
[30] C. D'Cruz and J. K. Pachos, Chiral phase from three-spin interactions in an optical lattice, Phys. Rev. A **72**, 043608 (2005).
[31] See Supplemental Material at http://link.aps.org/supplemental/10.1103/PhysRevLett.130.016701 for a full derivation of all results obtained from mean field theory and a further discussion of the conditions required for thermalization in the model.
[32] H. Nielsen and M. Ninomiya, A no-go theorem for regularizing chiral fermions, Phys. Lett. **105B**, 219 (1981).
[33] H. Nielsen and M. Ninomiya, Absence of neutrinos on a lattice: (ii). Intuitive topological proof, Nucl. Phys. **B193**, 173 (1981).
[34] E. Tirrito, M. Lewenstein, and A. Bermudez, Topological chiral currents in the Gross-Neveu model extension, Phys. Rev. B **106**, 045147 (2022).
[35] G. E. Volovik, *The Universe in a Helium Droplet*, 2nd ed. (Clarendon Press, Oxford, 2003), p. 424.

[36] U. Schollwöck, The density-matrix renormalization group in the age of matrix product states, Ann. Phys. (Amsterdam) **326**, 96 (2011).
[37] P. Calabrese and J. Cardy, Entanglement entropy and quantum field theory, J. Stat. Mech. (2004) P06002.
[38] T. Giamarchi, *Quantum Physics in One Dimension* (Oxford University Press, New York, 2003), p. 29.
[39] E. Miranda, Introduction to bosonization, Braz. J. Phys. **33** (2002).
[40] S. Aditya and D. Sen, Bosonization study of a generalized statistics model with four Fermi points, Phys. Rev. B **103**, 235162 (2021).
[41] J. Haegeman, T. J. Osborne, and F. Verstraete, Post-matrix product state methods: To tangent space and beyond, Phys. Rev. B **88**, 075133 (2013).
[42] G. E. Volovik, *The Universe in a Helium Droplet* (Oxford University Press, New York, 2009), Chap. 32.
[43] M. Perarnau-Llobet, A. Riera, R. Gallego, H. Wilming, and J. Eisert, Work and entropy production in generalised Gibbs ensembles, New J. Phys. **18**, 123035 (2016).
[44] L. Vidmar and M. Rigol, Generalized Gibbs ensemble in integrable lattice models, J. Stat. Mech. (2016) 064007.
[45] M. Srednicki, Chaos and quantum thermalization, Phys. Rev. E **50**, 888 (1994).
[46] J. M. Deutsch, Quantum statistical mechanics in a closed system, Phys. Rev. A **43**, 2046 (1991).
[47] M. Rigol, V. Dunjko, and M. Olshanii, Thermalization and its mechanism for generic isolated quantum systems, Nature (London) **452**, 854 (2008).
[48] D. Jaksch, C. Bruder, J. I. Cirac, C. W. Gardiner, and P. Zoller, Cold Bosonic Atoms in Optical Lattices, Phys. Rev. Lett. **81**, 3108 (1998).